Agricultural and Forest Meteorology 376 (2026) 110885

Contents lists available at ScienceDirect

Agricultural and Forest Meteorology

journal homepage: www.elsevier.com/locate/agrformet

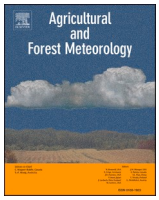

An investigation of corrective approaches for uncertain winds and analysis of impacts on smoke model performance

Zongrun Li [a], Susan M. O'Neill [b], Rime El Asmar [c], Yongtao Hu [a], Adam K. Kochanski [d], Angel Farguell [d], Jan Mandel [e], David J. Tanner [c], L. Gregory Huey [c], Armistead G. Russell [a], Rodney J. Weber [c], M. Talat Odman [a,*]

[a] School of Civil and Environmental Engineering, Georgia Institute of Technology, Atlanta, GA 30332, USA
[b] United States Department of Agriculture Forest Service, Pacific Northwest Research Station, Seattle, WA, USA
[c] School of Earth and Atmospheric Sciences, Georgia Institute of Technology, Atlanta, GA 30332, USA
[d] Wildfire Interdisciplinary Research Center, San José State University, San Jose, CA, USA
[e] Department of Mathematical and Statistical Sciences, University of Colorado Denver, Denver, CO, USA

ARTICLE INFO

Keywords:
Prescribed fires
Smoke modeling
Wind bias
Evaluation methods
Fire modeling

ABSTRACT

In wildland fires, wind affects fire propagation, emission intensity, and smoke transport; therefore, uncertainties in wind simulations can critically impact $PM_{2.5}$ concentration produced by coupled fire-atmosphere models or chemical transport models. These uncertainties must be addressed prior to assessing other parameters that may affect model-predicted $PM_{2.5}$ concentrations through comparisons with observations. This study simulated prescribed fire events with accurate ignition pattern design and high spatial-temporal resolutions using the coupled fire-atmosphere model WRF-SFIRE. We designed, implemented, and evaluated various wind bias reduction and smoke model evaluation methods to quantitatively capture the impacts of wind uncertainty on simulated smoke concentrations. For the wind bias reduction methods, incorporating wind observations into initial and boundary conditions proved effective in reducing bias, especially for wind speed. The suggested method resulted in RMSE values of 63 degrees for wind direction and 0.5 m/s for wind speed, lower than the standard WRF nudging benchmark's 71 degrees and 1.5 m/s, respectively. This improvement in wind simulation accuracy enhanced the smoke simulation performance, successfully identifying 5 out of 8 detected $PM_{2.5}$ peaks ($\geq$ 35 $\mu g/m^3$) missed in the benchmark WRF simulation using nudging. Among smoke model evaluation methods, which are post-analysis algorithms on the numerical modeling results, the equal time backward/forward trajectory method was the most effective approach. It successfully captured 7 $PM_{2.5}$ peaks, which were not well simulated in the nudging benchmark. These smoke evaluation methods estimated uncertainty in smoke concentration by considering the simulated wind bias and demonstrated that the smoke concentration simulation is highly sensitive to the wind bias from the wind simulation. This study is unique in suggesting novel solutions to improving modeled wind field data and creative approaches to post-analysis of smoke transport simulations.

1. Introduction

Wildfires, which are unplanned and uncontrolled vegetation-burning events, have adverse effects on human health and wealth. In recent years, wildfire intensity and frequency have increased in the United States (Jaffe et al., 2020; Dennison et al., 2014), and the trend is expected to continue due to global warming (Liu et al., 2013; Diffenbaugh et al., 2021; Jolly et al., 2015; Burke et al., 2023). Prescribed fires are controlled, typically low(er)-intensity burns proposed as an effective land management strategy to decrease fuel load, promote ecosystem health, and reduce wildfire damage. However, both wildfire and prescribed fire degrade the air quality since a significant amount of air pollutants, such as particulate matter (PM), volatile organic compound (VOC), and nitric oxide and nitrogen dioxide (NO_x), are emitted during both flaming and smoldering phases of combustion (Prichard et al., 2020). To assess the air quality impacts induced by wildland fires, which are critical for public health studies and policy making, numerical models such as fire behavior models and chemical transport models are

* Corresponding author.
E-mail address: odman@gatech.edu (M.T. Odman).

https://doi.org/10.1016/j.agrformet.2025.110885
Received 12 March 2025; Received in revised form 25 August 2025; Accepted 6 October 2025
Available online 21 October 2025

implemented to provide spatial-temporal smoke predictions (Chen et al., 2021; Matz et al., 2020). Fire and smoke simulations are also essential for fire management, helping fire managers make decisions about prescribed fires and plan experimental field studies (Kochanski et al., 2018).

WRF-SFIRE (Mandel et al., 2014; Mandel et al., 2011) is a fire behavior model incorporated in Weather Research and Forecasting Model (WRF) (Skamarock et al., 2019), which simulates fire propagation and smoke transport. The chemistry mechanism can also be considered by coupling with WRF-Chem (Kochanski et al., 2016). Unlike typical chemical transport models, such as Community Multiscale Air Quality Modeling (CMAQ) (Byun and Schere, 2006) or Comprehensive Air Quality Model with Extensions (CAMx) (Emery et al., 2024), which utilize the pre-processed meteorological fields and fire emissions, the WRF-SFIRE considers the coupling effects between atmosphere and fire (Mandel et al., 2011; Beer, 1991). The model simulates fire-modified meteorology and fire propagation under specific meteorological conditions. The emissions and vertical plume distribution due to pyro-convection are calculated online based on simulated local meteorology and fire behavior. Previous studies showed that the WRF-SFIRE could be conducted to simulate the fire propagation and air quality impacts for both wildfires (Kumar et al., 2024; Lu et al., 2012; Kochanski et al., 2019; Mallia et al., 2020) and prescribed fires (Mallia et al., 2020; Mallia et al., 2018) under desired ignition patterns.

Emission estimations and meteorology are the fundamental factors impacting air quality simulations and primary sources of uncertainties. Many studies focused on the impact of emission uncertainty on air quality modeling, particularly in long-term and large-scale simulations (Tian et al., 2009; Carter et al., 2019; Su et al., 2023). For instance, Carter et al. (Carter et al., 2019) simulated black carbon and organic carbon concentrations using different fire emission inventories, including Global Fire Emissions Database (GFEDv4s) (Giglio et al., 2013), Fire Inventory from NCAR (FINNv1.5) (Wiedinmyer et al., 2011), Quick Fire Emissions Dataset (QFEDv2.4) (Koster et al., 2015), and Global Fire Assimilation System (GFASv1.2) (Kaiser et al., 2012), over North America from 2004 to 2016. The uncertainty in the fire emissions could lead to 0.5 to 1.6 $\mu g/m^3$ differences in annual population-weighted $PM_{2.5}$. Liu et al. (Liu et al., 2020) conducted an adjoint monthly GEOS-Chem simulation for the Indonesia region with different fire emission inventories, including GFEDv4s, FINNv1.5, GFASv1.2, QFEDv2.5r1, and Fire Energetics and Emissions Research (FEERv1.0-G1.2) (Ellison et al., 2014) from 2003 to 2016. Although smoke simulations using different fire inventories were correlated (correlation ranging from 0.64 to 0.84), the magnitude of mean smoke $PM_{2.5}$ during the burning season (July to October) varied across inventories by >20 $\mu g/m^3$ (>500 %). In these studies, the effects of heterogeneous meteorological conditions, like wind direction, tend to average out and become less important compared to the regional high spatial-temporal simulations.

Meteorological conditions, especially winds, are essential in hourly (sub-hourly) small/smaller-domain fire simulations and are rarely addressed. Li et al. (Li et al., 2020) offered a powerful analysis quantifying the orders of magnitude differences in smoke modeling results due to an ensemble of parameter variations, one of which is the meteorological datasets. Smoke dispersion paths were strikingly different between simulations using the North American Model (NAM) (NCAR 2015), the North American Regional Reanalysis (NARR) (NCAR 2005), and the Global Data Assimilation System (GDAS) (NCAR 2015) meteorological datasets (see their Fig. 5). Potter et al. (Potter et al., 2023) discussed how measured and modeled winds can be quite different, a finding also reported by some previous studies (Kumar et al., 2024; El Asmar et al., 2024). The discrepancies between modeled and measured winds arise from factors such as model averaging (spatial and temporal), model physics (e.g., mass conservation), and measurement technology, including how the measured data are averaged/quantified. Model wind data are an average representative value for the grid cell and thus are not necessarily representative of the measured winds at a point in the grid cell. Measured winds change much more frequently than modeled and include gusts that the modeling system does not capture. Thus, modeled data tend to be much smoother and do not have the fluctuations present in measurements. Miller et al. (Miller et al., 2019) conducted a detailed comparison of modeled and measured winds during smoke intrusions in central Oregon and found that daytime mean wind error was approximately 40 degrees, and at night, the error went up to approximately 80 degrees. The meteorological model also tended to overestimate wind speeds. These variabilities have dramatic effects on smoke transport, and these studies highlight the critical importance wind plays in smoke dispersion modeling and the nuances to be aware of with both modeled and measured wind data. Large questions remain about how to account for or correct meteorological wind fields to improve smoke transport modeling.

Additionally, in fire-atmosphere models, fire propagation, emission, and smoke transport are all interconnected, highlighting the importance of an accurate representation of winds. Unfortunately, very few studies have discussed the impact of wind uncertainty on concentration simulations with traditional chemical transport models or coupled fire-atmosphere models. Yang et al. (Yang et al., 2011) discussed the impact of wind on concentration uncertainties by using trajectory models with different meteorological datasets. The forward trajectory results indicated that the smoke-impacted region had significant discrepancies under different meteorology inputs. However, the study did not quantitatively show the wind impacts on the concentration uncertainty. Menendez and coauthors conducted a sensitivity analysis on wind impacts for CMAQ simulations (Garcia-Menendez et al., 2013) by applying body-solid rotations to adjust wind direction by $\pm$ 5°, $\pm$10° and $\pm$30°, and scaling wind speed by $\pm$ 10 %, $\pm$ 20 % and $\pm$ 30 % individually in the Meteorology-Chemistry Interface Processor (MCIP) (Byun et al., 1999), which provides the meteorological inputs for the CMAQ model. Then, the study simulated the concentration using CMAQ under these 12 perturbed wind fields to quantitatively demonstrate the impact of wind on concentration levels. This method, although promising, cannot be directly used for the coupled fire-atmosphere models, which simulate the wind along with the fire simulation instead of using pre-processed meteorological conditions. Additionally, the study did not discuss how to mitigate the wind bias using the method or consider the wind bias when comparing the concentration simulations with observational data.

This study consists of two parts. The first part examined various wind bias reduction methods aimed at minimizing wind bias in meteorological simulations. These methods include data assimilation with wind observations or interpolated observation data, as well as adjustments to initial and boundary conditions. While these approaches reduce wind bias, they cannot eliminate it. As a result, residual wind bias must still be considered when evaluating smoke model performance. To address this, in the second part, we developed and implemented smoke model evaluation methods to quantitatively assess wind impacts on smoke simulations. These methods account for differences between observed and simulated winds, providing a measure of uncertainty in the simulation results. The wind bias reduction and smoke model evaluation methods presented in this study are applicable to other chemical transport models, such as CMAQ and WRF-Chem, for fire-related case studies.

2. Measurements and modeling frameworks

2.1. Prescribed fires and measurements

In this study, we focused on three prescribed burns conducted at Fort Stewart Army Base in eastern Georgia, United States, on March 2nd, March 3rd, and March 5th, 2022. The prescribed burn boundaries are shown in Fig. 1, and the location of Fort Stewart Army Base in Georgia is indicated in Figure S1. Burn units F6.4 and F6.3 were burned separately on March 2nd and March 3rd. Burn units E16.2 and E16.3 were burned together on March 5th. The prescribed burns were ignited using the

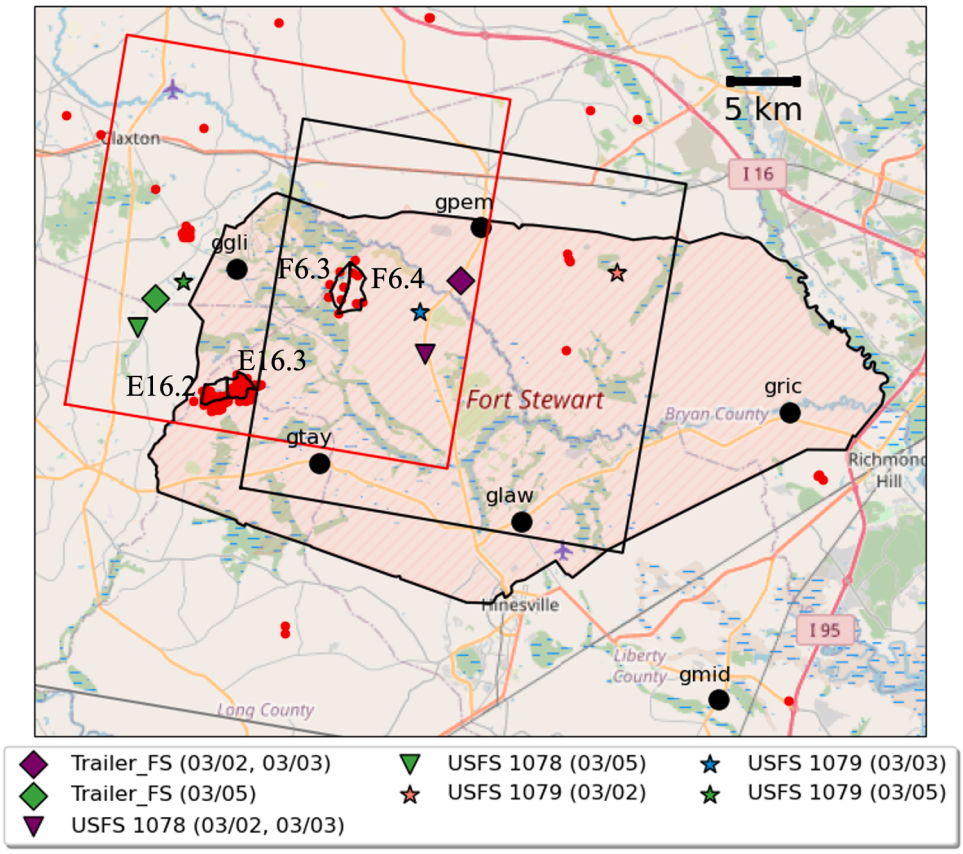

Fig. 1. Monitor locations, prescribed burned units, and WRF-SFIRE simulation domains. Measurements dates (MMDD) are given for the Trailer and USFS monitors. The red dots show the Fire Radiative Power (FRP) detections from the Fire Information for Resource Management System (FIRMS) (FIRMS, 2022), which includes active fire products from Terra MODIS, Aqua MODIS, Suomi-NPP VIIRS, and NOAA-20 VIIRS. The polygons aligned with the FRP detections are the prescribed burned units analyzed in this study.

aerial ignition method, which utilized a helicopter to drop incendiary chemical-filled ping-pong balls. The helicopter's Global Positioning System (GPS) recorded the incendiary objects' drop positions. To prevent the fire from escaping out of the designed boundary, firebreaks were set before the prescribed burn was conducted. This was done by first burning the fuels along the boundaries for perimeter control. To measure the transported smoke and evaluate the modeling performance, we employed a mobile air quality monitoring trailer that included a tapered element oscillating microbalance (TEOM) (El Asmar et al., 2024; El Asmar et al., 2025) (square symbol in Fig. 1), and two portable Met One Instruments Inc. Environmental Beta Attenuation Monitors (EBAM) (Instruments, 2022) USFS 1078 and USFS 1079 provided by US Forest Service (USFS) (shown as triangle and star symbols, respectively in Fig. 1) to collect $PM_{2.5}$ concentration data during prescribed burns. The monitors were placed in Fort Stewart on March 2nd and 3rd to capture the smoke from F6.3 and F6.4 as it was transported by the westerly winds. Then, on March 5th, the monitors were relocated outside Fort Stewart to capture the smoke coming from E16.2 and E16.3 under southeasterly winds. These monitors measure $PM_{2.5}$ at a 1-minute internal sampling frequency, and we averaged the data to 1-hour. Since the relative humidity (RH) conditions affect EBAM $PM_{2.5}$ performance (Schweizer et al., 2016; Zachariassen, 2003), especially at ambient RH levels greater than 65 %, we excluded EBAM $PM_{2.5}$ measurements collected during periods when RH exceeded this threshold before computing the hourly averages. We collected wind measurements at a 2-m height from Remote Automatic Weather Stations (RAWS) monitors (Center, 2008) located in or near Fort Stewart, including Glisson's Pond (ggli), Lawson (glaw), Midway (gmid), Taylor's Creek (gtay), Pembroke (gpem), and Richmond Hill (gric) (shown as circles in Fig. 1). The wind data from RAWS is collected in 10-minute mean values prior to data transmission (Zachariassen, 2003). The data we used were downloaded directly from the RAWS USA Climate Archive (DRI, 2024), which provides wind data already averaged to 1-hour intervals. As indicated in the RAWS review report (Zachariassen, 2003), wind speed is truncated to whole numbers before transmission (e.g., 6.9 mph becomes 6.0), potentially underestimating values by up to ~1 mph (0.4 m/s). We also collected wind measurements from EBAM USFS 1079, which was equipped with a Met One Instruments anemometer model EX-034 mounted on the EBAM tripod at a height of 1.5-m. The internal sampling frequency of the wind measurements is 1-minute, and the data were averaged to 1-hour. Since WRF uses 10-m wind for data assimilation and simulates the surface wind at 10-m, we used the log wind profile (Holmes, 2015) formula (shown in Text S1) to convert the 2-m wind measurements to 10-m wind. We used a surface roughness length of 0.03 m (Holmes et al., 2007) in the log wind profile formula, which corresponds to typical grassland conditions. Locations of measurement platforms are presented in Fig. 1.

2.2. *Wind and $PM_{2.5}$ simulations*

First, we simulated meteorological conditions for the study using WRF version 4.2 (Skamarock et al., 2019). The simulation period was from March 1st at 0 UTC (February 28th at 19:00 local time) to March 7th at 0 UTC (March 6th at 19:00 local time), which covered all the prescribed burning events. The simulation was started one day before the burns to spin up the model. The WRF model used one-way coupling and included three domains with 12 km, 4 km, and 1 km resolutions (Figure S2). The initial and boundary conditions for the outermost 12

km domain came from the NAM 12 km model (NCAR 2015). The National Land Cover Database (NLCD) (Homer et al., 2012) was used to provide the static geographical data. In our benchmark simulations, we utilized the WRF model with and without data assimilation (nudging) (Reen, 2016), a standard approach for establishing meteorological conditions for air quality simulations. In this study, the data assimilation case utilized the grid nudging and observational nudging with National Centers for Environmental Prediction (NCEP) global surface and upper air observational weather data (NCAR 2004; NCAR 2004), deployed EBAM monitor measurements, and measurements from selected RAWS stations (parameters used for wind nudging are shown in Table S1).

Then, we used WRF-SFIRE (Mandel et al., 2011) (version 4.2) to simulate the fire evolution, plume rise, and smoke dispersion and analyze the impact of assimilated winds on fire and smoke dispersion simulations. WRF-SFIRE is a coupled-atmosphere model, which considers the interactions between the atmosphere and fire since they mutually influence each other during the fire spread. The fire spread rates in WRF-SFIRE are calculated by the Rothermel formula (Rothermel, 1972). The formula estimates the rate of spread of the surface fire's flaming front based on fuel types, fuel moisture, slope, and wind speed. An external 1 km weather simulation performed with WRF provided the meteorological initial and boundary conditions. The WRF-SFIRE model includes a fuel moisture component that is driven by the simulated weather fields (Mandel et al., 2014; Vejmelka et al., 2016). This integration provides real-time fuel moisture data essential for determining the spread rate of fires. Since the WRF-SFIRE model requires high spatial resolution for simulating fire spread under heterogeneous fuel conditions, we used a 200 m atmospheric resolution with a subgrid ratio of 10, resulting in a fire model resolution of 20 m. A 3D scale-adaptive turbulent kinetic energy scheme (Zhang et al., 2018) is conducted for the 200 m domain to resolve the "gray zone" issue (Honnert et al., 2020) in turbulence, where the grid resolution is too fine for traditional large-scale modeling but too coarse for resolving small-scale turbulence. The 30 m-resolution LANDFIRE product provided the elevation data and 13 Anderson fire behavior fuel type data (Department of the Interior, G.S., and U.S. Department of Agriculture. LANDFIRE 2016). For simulating the $PM_{2.5}$ concentrations, we utilized the $PM_{2.5}$ inert tracer in WRF-SFIRE, assuming the secondary $PM_{2.5}$ formation would be negligible since the monitor location was near the burn units, but this may underestimate $PM_{2.5}$ mass concentration during photochemically active periods and when smoke ages beyond 1 h (El Asmar et al., 2025). We designed two different simulation domains, both with 145 west-east by 140 south-north grid points, as shown in Fig. 1, to capture the smoke trajectories. The black frame shows the fire simulation domain on March 2nd and March 3rd. The red frame shows the simulation domain for the March 5th prescribed fire. We set the emission factor for each fuel type based on the Smoke Emission Reference Application (SERA) (Prichard et al., 2020) (Table S2). The aerial ignitions during the Fort Stewart burns were represented in the model by initializing the fire arrival time (TIGN_G). The value of the fire arrival time variable was updated for each subgrid cell in the WRF-SFIRE input file according to GPS-recorded ignition time (ignition patterns are shown in Figures S3-S5). First, we identified the subgrid cells corresponding to each incendiary object's drop position using the nearest grid match. Then, we assigned the drop timing of the incendiary object to the subgrid cell. We also removed the fuel outside the fire boundaries in the input to avoid the fire spreading out of the boundaries (applied fuel types and elevation are shown in Figures S6-S8). The simulated concentration was compared with the measured $PM_{2.5}$ to evaluate the model performance. The fuel moisture model was activated during the WRF-SFIRE simulations, and the ground fuel moisture content was initialized as zeros at the beginning of the simulation hour 0 UTC for each burn date.

3. Methods

In this study, we designed and implemented various methods to reduce the uncertainties in wind fields and to investigate the impacts of uncertain winds on smoke simulations related to prescribed fires (Table 1). First, two benchmark simulations, one without (B) and one with nudging (NB), were conducted. These benchmarks provided the meteorological initial and boundary conditions for the coupled fire-atmosphere model WRF-SFIRE, and they were used in measuring the performance of the new methods. The two categories of methods discussed here are: i) wind bias reduction and ii) smoke model evaluation methods. The wind bias reduction methods include 1) adjusting the initial and boundary condition inputs to WRF-SFIRE (AICBC) and 2) augmenting the assimilation data set by interpolating observational data for nudging the WRF-SFIRE solution towards observations (AN). The smoke model evaluation methods are based on statistical analysis after the WRF-SFIRE simulations, including rotation and translation (RT), equal time backward/forward trajectory (ETBFT), and equal distance backward/forward trajectory (EDBFT) methods. All these methods were implemented to find the pseudo-monitor location, which is the projection of the actual monitor location considering the uncertainties in simulated winds. For example, suppose the measured wind indicates that the smoke directly hit the monitor, but the bias in the modeled wind directs the smoke away from the monitor. The pseudo-monitor location in such a situation is directly downwind according to the simulated wind field. Instead of comparing the monitoring concentration with the simulated concentration at the actual monitor location, the smoke model evaluation method uses the simulated concentration at the pseudo-monitor location.

3.1. Methods for mitigating wind biases

The AICBC and AN methods, as wind bias reduction methods, are summarized in Table 1, and each is discussed in detail below.

3.1.1. Adjusted initial and boundary conditions (AICBC)

In this method, we adjusted the wind initial and boundary conditions (IC/BC) that are input to WRF-SFIRE by using wind observations. For this, we revised the wind field simulated by WRF over the parent domain to minimize the disparities between observed and modeled winds. First, we performed a scaling and solid-body rotation on the WRF wind field

Table 1
Method names and short descriptions.

Method Categories	Method Name	Description
Benchmarks	Benchmark (B)	WRF-SFIRE with initial and boundary conditions (IC/BC) provided by 1-km resolution WRF
	Nudging Benchmark (NB)	WRF-SFIRE with nudging and IC/BC provided by 1-km resolution, nudged WRF
Wind Bias Reduction Methods	Adjusted Initial and Boundary Conditions (AICBC)	WRF-SFIRE with IC/BC from wind fields rotated and scaled according to wind direction and wind speed biases
	Augmentation Nudging (AN)	WRF-SFIRE with nudging to observational data augmented by interpolation
Smoke Model Evaluation Methods	Rotation and Translation (RT)	Rotating and translating the monitor location according to wind biases to find evaluation locations
	Equal Time Back/forward Trajectory (ETBFT)	Computing backward and forward trajectories of equal time to find evaluation locations
	Equal Distance Back/forward Trajectory (EDBFT)	Computing backward and forward trajectories of equal distance to determine evaluation locations

simulated over the 1-km resolution parent domain. The rotation degree and the scaling factor were calculated from the averaged wind direction bias and wind speed bias between the 1 km resolution WRF simulation and observations at meteorology stations (the process is described in more detail in Text S1 Adjusted Initial and Boundary Conditions Method section). Accordingly, the metgrid data, which has a combination of geography and meteorological data processed by WRF Pre-Processing System (WPS), are modified. Then, adjusted initial and boundary conditions for WRF-SFIRE were generated with the modified data.

3.1.2. Augmentation nudging (AN)

Observational nudging is a method to introduce artificial tendency terms in WRF simulations, which gradually nudge the model around the observation stations towards corresponding observations (Reen, 2016). However, for case studies involving prescribed fires, the observation stations are spatially sparse, as the study area is typically rural. Additionally, since WRF-SFIRE is generally used with a high spatial resolution (~200 m) for computational efficiency, the typical simulation domain is small, with limited observation monitors. Also, the nudging method, when using the default settings (Table S1), nudges the simulation with slight intensity in each time step to avoid inducing unrealistic results. However, it cannot mitigate all the wind bias for a typical one-day prescribed fire event simulation. One possible mitigation method is to increase the nudging intensity by tuning the nudging parameters, including the radius of influence and the nudging time scale, which was discussed in previous studies (Bowden et al., 2012; Spero et al., 2018). In this study, instead of tuning the nudging parameters, we enhanced the observational data through interpolation to address the challenge of insufficient monitoring data in small fire simulation domains by leveraging data from the parent domain's monitors. First, we generated a 1-km resolution wind field by applying Kriging interpolation (Murphy, 2014; Oliver and Webster, 1990) to the observed u-wind and v-wind data from selected meteorological monitors. Then, we extracted the wind data from each grid cell of the 1-km resolution interpolated observational field and created an augmented observation dataset over the WRF-SFIRE domain. This dataset was then used as the observational nudging input to the WRF-SFIRE simulation (the process is described in more detail in Text S1 Augmentation Nudging Method section).

3.2. Methods for smoke model evaluation under uncertain winds

Since wind biases are commonly found in meteorological simulations, even when wind reduction methods are applied, they must still be considered in smoke model evaluation. Smoke model evaluation methods below quantify the uncertainty in smoke concentration caused by wind biases. These methods are summarized in Table 1 and discussed in detail below.

3.2.1. Rotation and translation method (RT)

The idea behind the rotation and translation method is similar to that of the AICBC method above. Instead of conducting solid-body rotation and scaling of the wind field to correct the initial and boundary conditions, we calculated pseudo-monitor locations using the wind bias. Also, unlike considering the spatially averaged wind bias across the simulation domain, as done in AICBC, this method focuses on the wind bias at the monitor location. Some concentration monitors are not paired with collocated wind-measuring anemometers. We assumed the wind bias at such concentration monitoring locations to be the same as that at the nearest wind monitor (the assignments are listed in Table S3). To mitigate the effect of the wind direction bias on the trajectory of the smoke plume, we rotated the monitor location around the centroid of the burn unit by an angle equal to the hourly wind direction bias at the selected monitor (Figure S9 is the conceptual figure for explanation). To mitigate the effect of the wind speed bias on the smoke impact timing, we translated the monitor location by the distance that the smoke would travel due to the hourly wind speed bias. By combining these two processes, we calculated a pseudo-monitor location for a specific wind direction bias and wind speed bias at each hour (details on rotation and translation operations are provided in Text S1 Rotation and Translation Method section). However, the concentration field during a specific hour was not only affected by the wind field at that hour but also by the wind fields at previous hours, since all the wind vectors along the trajectory consecutively act on the smoke plume during its transport. To address this uncertainty, we spanned the ranges of wind direction and speed biases from the current and previous hours and calculated the pseudo-monitor locations for all the combinations in the range. For example, assuming wind direction and speed biases at hour t are $\sigma_{dir}(t)$ and $\sigma_{spd}(t)$, to estimate the wind uncertainty impacts on concentration at time t, we considered all the combinations of wind direction and speed biases in the following range:

$$\left[\min(\sigma_{dir}(t-1),\ \sigma_{dir}(t)), \max(\sigma_{dir}(t-1),\ \sigma_{dir}(t))\right] \times \left[\min\left(\sigma_{spd}(t-1),\ \sigma_{spd}(t)\right), \max\left(\sigma_{spd}(t-1),\ \sigma_{spd}(t)\right)\right] \quad (1)$$

where the symbol $\times$ represents the Cartesian product. We calculated the pseudo-monitor locations for each wind bias in this range and all possible concentrations at these pseudo-monitor locations.

3.2.2. Equal time (ETBFT) and equal distance (EDBFT) backward/forward trajectory methods

The trajectory methods included backward and forward trajectory steps to find the pseudo-monitor location (Fig. 2). In the backward trajectory step, we started from the concentration monitor location and aimed at finding the source of measured smoke using the observed wind. Since there is no continuous spatial field of wind observations, the winds along the backward trajectory needed to be estimated. We assumed the observed winds along the trajectory had a Gaussian distribution, in which the mean value was the measured wind at the concentration monitor location (if there were no collocated wind measurements at the concentration monitor, we assigned the wind at the nearest wind measuring monitor as the mean) and the variance was the spatial variance at the current hour among the wind monitors over the WRF-SFIRE domain. The trajectory continued until the closest location to the burn units. These locations were assumed to be the source of the smoke and used as the starting point for the forward trajectory step. To find the pseudo-monitor location, i.e., the projection of the monitor location under the simulated wind field, we calculated the forward trajectory with the wind field simulated by WRF-SFIRE.

The first method, equal time backward/forward trajectory (ETBFT), calculated the forward trajectory using the same period as the backward trajectory. This method would conceptually mitigate the impact of uncertainties in simulated winds on smoke transport. However, the disparities of smoke diffusion between reality and simulation due to the wind speed bias were not addressed by this method. For example, higher wind speed in the simulation compared to the real world would not only affect the timing of the smoke hitting the monitor but also dilute the intensity of the smoke. An alternative method, equal distance backward/forward trajectory (EDBFT), was implemented based on the assumption that the diffusion of the smoke was related to the transport distance. So, the forward trajectory for a period that resulted in the minimal difference between the smoke travel distance and the backward trajectory distance was used (technical and mathematical details of both methods are provided in Text S1).

To estimate the uncertainty in the backward trajectory step, we conducted a Monte Carlo simulation and created 1000 trajectory samples assuming Gaussian distributions for u and v winds. For each backward trajectory sample, we calculated the forward trajectory to find a pseudo-monitor location and extracted the concentration at that location. The 1-sigma concentration range (which refers to the 16th and 84th percentiles, or one standard deviation below and above the mean in a Gaussian distribution) at pseudo-monitor locations from all samples

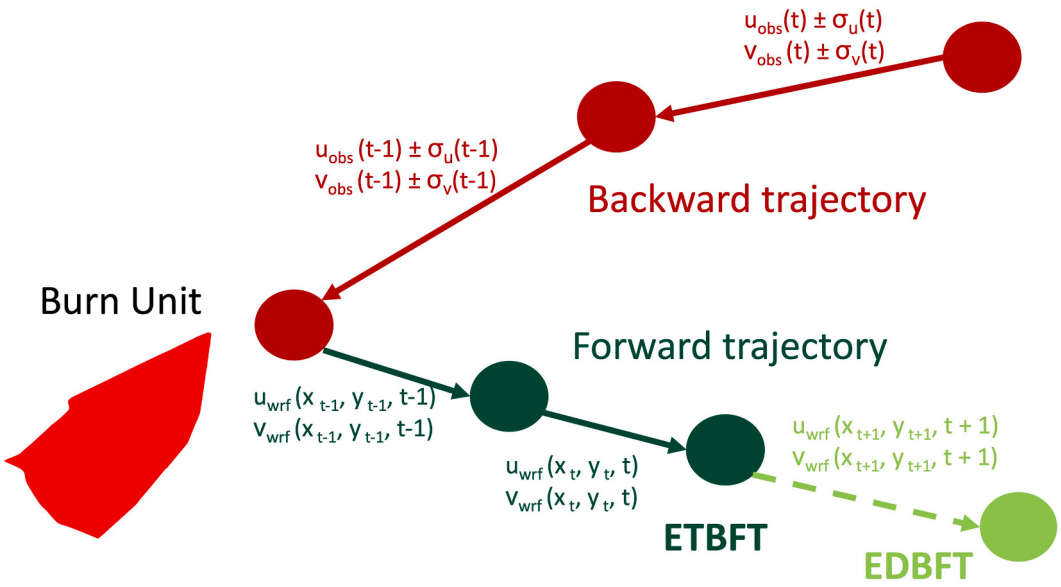

Fig. 2. Representation of equal time and equal distance backward/forward trajectory methods. The differences between the equal time trajectory (dark green) and the equal distance trajectory (light green) are in the forward trajectory step.

covered the uncertainty in concentration caused by variable winds.

4. Results

In this section, we first present the wind and smoke simulation performances of the two benchmarks, B and NB. The WRF modeling results of these benchmarks at 1-km resolution are used by the wind bias reduction methods and provide IC/BC to smoke simulations at 200 m resolution. The effectiveness of wind bias reduction methods is evaluated by comparing them with NB at 200 m resolution. Additionally, we analyzed the smoke simulations of NB at 200 m resolution to illustrate the impacts of biased winds by using smoke model evaluation methods.

4.1. Benchmark wind and smoke simulations

We compared WRF simulated winds at 12 km, 4 km, and 1 km resolutions with hourly surface wind measurements from Techniques Development Laboratory (TDL) (Commerce 1987), our measurements, and selected RAWS stations. The model performance was assessed using statistical metrics (formulas provided in Text S2) calculated between observed and simulated winds on March 2nd, March 3rd, and March 5th, which were prescribed burning dates. The simulation performance of surface wind direction and wind speed was evaluated under different statistical metrics (Tables S4 and S5), and the method for calculating wind speed and direction bias was detailed in Text S3. For the overall wind modeling performance, we used the Taylor diagram (Figure S10), which combines the model's standard deviation, centered root mean square error (CRMSE), and correlation with observations in a single plot for model evaluation (Taylor, 2001). The distance between any model's point and the observation indicates the performance of the model, with the performance being better with a shorter distance. For the wind direction and wind speed, the Taylor diagram indicated that NB and B showed a similar performance at 12 km and 4 km domains. NB showed improvements over B in wind simulations, especially on wind speed in the 1 km domain. However, the hourly wind simulation from NB in the 1 km domain still showed poor performance, especially on wind speed simulations, where the correlation was 0.34. Although the simulated wind direction in the 1 km domain correlated with observations (r = 0.88), the root mean square error (RMSE) was 71 degrees. The subpar performance can partly be attributed to the NCEP meteorological data used for nudging, which was reported every three hours, whereas the model was evaluated using hourly wind measurements. When we used these 1 km resolution benchmark meteorological simulations to provide ICBCs, wind simulations in B and NB at 200 m resolution showed bias compared to observations during the prescribed burning periods. NB showed slight improvements in both wind direction and speed compared to B (Fig. 3). However, both benchmarks displayed wind direction RMSEs higher than 71 degrees (Table S6) and wind speed RMSEs higher than 1.5 m/s (Table S7). The relatively low accuracy of wind simulation raised concerns about the performance of smoke simulations. Under such biased wind simulations, B (Figure S11) and NB's (Figure S12) smoke simulations failed to capture the $PM_{2.5}$ peaks at Trailer on March 3rd and March 5th and at USFS 1078 on March 2nd. Also, the $PM_{2.5}$ peak at USFS 1079 on March 3rd was significantly underestimated in NB's smoke simulations.

4.2. Wind and concentration performance under different wind bias reduction methods

The wind bias reduction methods were dedicated to decreasing the wind simulation bias in the fire simulation domain to mitigate the uncertain wind effects on concentration simulations. We used the statistical metrics mentioned above (results are shown in Tables S6 and S7) and Taylor diagrams (Fig. 3) to evaluate wind bias reduction methods' performance (Emery et al., 2017; Emery et al., 2001) during the fire simulation period, from the prescribed fire start time to the end of the UTC day (19:00 local time). Wind bias reduction methods used IC/BC from B or NB at 1-km resolution and were compared with NB at 200-m to understand their effectiveness. The Taylor diagram indicated that the AICBC method was the most effective method among all the simulations, especially for improving the wind speed simulation (Fig. 3). Here, we mainly focused on the AICBC method with nudging. The performance of AICBC without nudging can be found in Tables S6 and S7. The AICBC method resulted in 12 % and 64 % decreases in the RMSE for the wind direction and wind speed compared to the NB. The effectiveness of the AICBC method can be explained by the fact that the method forced the initial and boundary conditions and, consequently, the simulation is closer to the observations instead of propagating the wind bias from the parent domain to the study domain. The nudging process also improved the wind simulation performance. For the AN, the mean error (ME) and RMSE of the wind direction and wind speed were slightly improved compared to the NB; however, the benefits from nudging were not

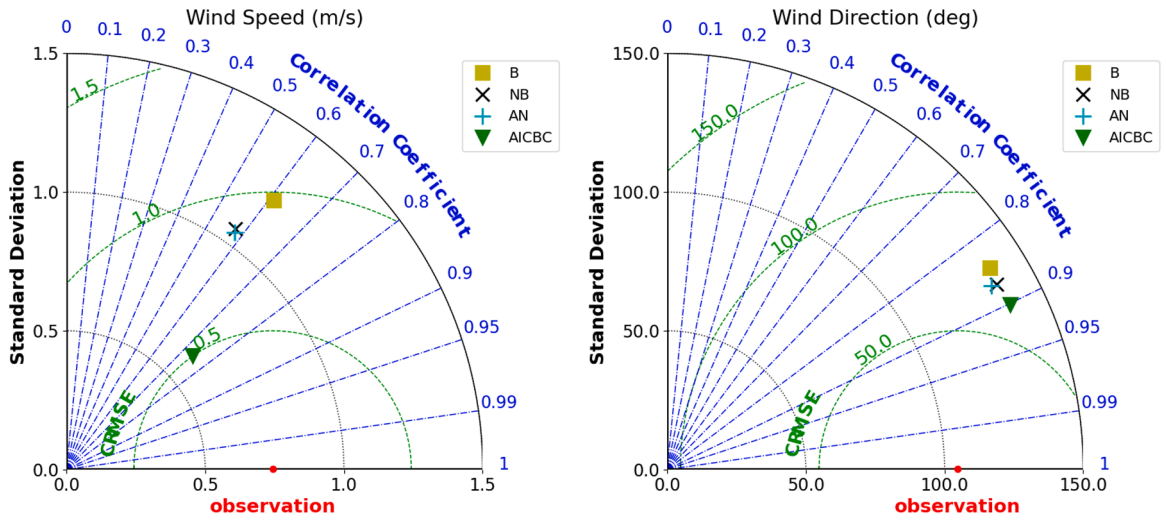

Fig. 3. Taylor diagrams of wind direction and wind speed. The red dot represents the observation, and the other symbols represent different model simulations.

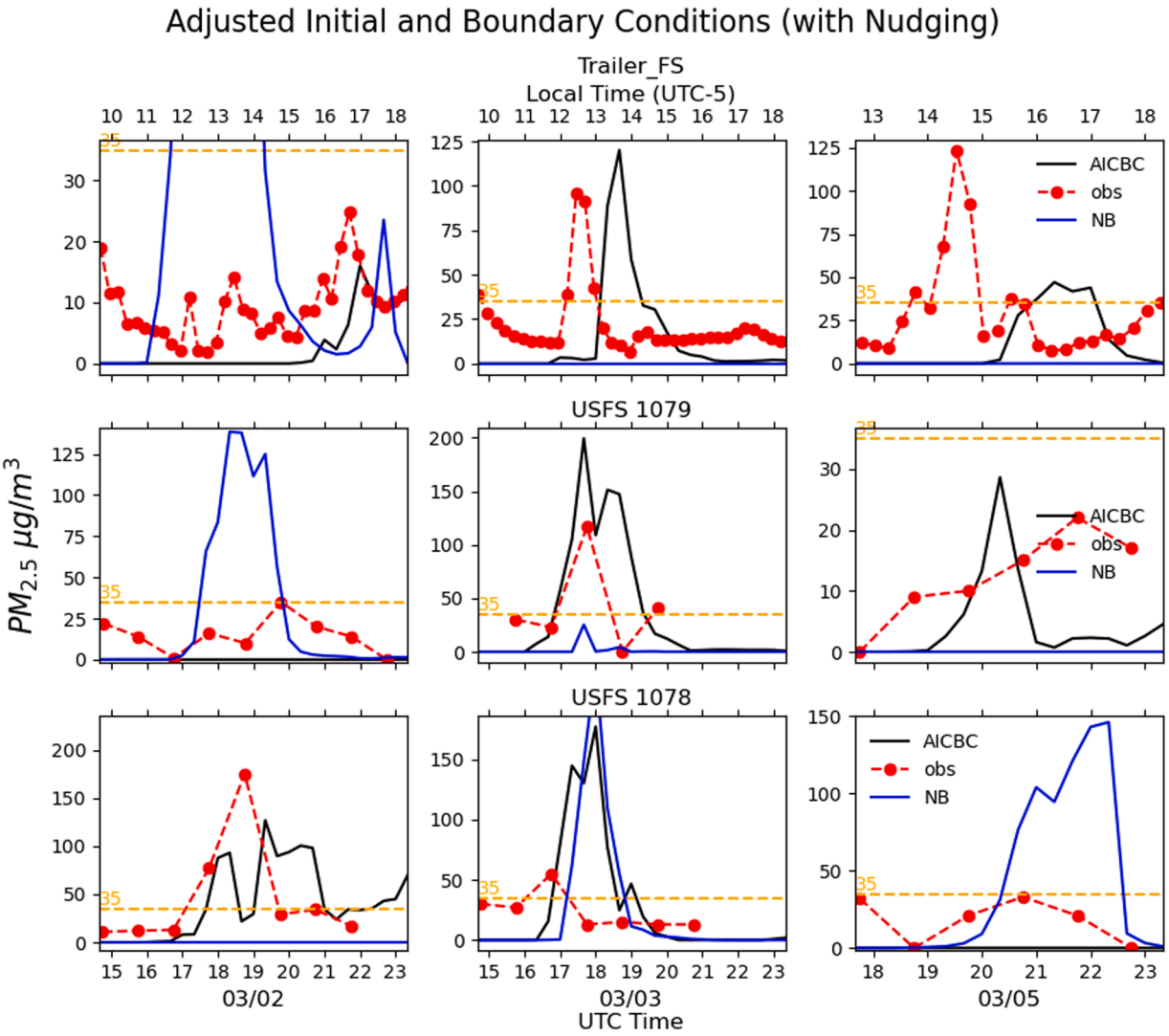

Fig. 4. Observed and simulated $PM_{2.5}$ concentration (AICBC with nudging) at Trailer FS (TEOM), USFS 1079 (EBAM), and USFS 1078 (EBAM) monitors on three prescribed fire days. The red dots with the dashed line, blue solid line, and black solid line indicate the observation, NB simulation, and AICBC simulation, respectively. The orange dashed line marks the 35 μg/m^3 $PM_{2.5}$ level, which is the daily standard in the U.S. (Agency, U.E.P 2012).

evident in this study. This could be because the nudging method nudged the model results to observation with a small perturbation term without tuning nudging parameters, and the correction intensity was kept low for each nudging step.

For the concentration evaluations, we compared the simulated concentrations with the concentrations observed after the prescribed fire was conducted (Fig. 4, Figures S13-S14). With the AICBC method (Fig. 4), which had the best wind simulation performance among all the methods, the smoke concentration simulation performance was improved compared to NB (Figure S12, also shown as black lines in Fig. 4), especially for capturing the smoke at Trailer FS and USFS 1078 on March 2nd, Trailer FS and USFS 1079 on March 3rd. On March 5th, the three monitors were close to each other, and the observations indicated that Trailer FS was more heavily impacted by the smoke compared to the other monitors around 19:30 UTC (14:30 local time), approximately one and a half hours after the ignition start time. However, all the simulations, including AICBC, failed to capture the high $PM_{2.5}$ peak at Trailer FS between 19:00 and 20:00 UTC (14:00 to 15:00 local time) on March 5th (an enlarged figure is shown in Figure S15). This can be explained by the slower fire spread rate and no obvious smoke in the model after the first 30 min of the fire (Figure S16). Although the model overestimated the wind speed, the fire propagated slowly since the fuel moisture was overestimated on March 5th (Figure S17). The almost doubled fuel moisture content in WRF-SFIRE on March 5th impeded the model from simulating the first $PM_{2.5}$ peak at Trailer FS. The AICBC with nudging simulated the peak starting around 20:40 UTC (15:40 local time) while the smoke impact lasted until 22:20 UTC (17:20 local time), much longer than the observed smoke impact. This can be explained by the high wind direction bias after 21:00 UTC (16:00 local time), which transports the smoke more westerly in the simulation (Figure S15).

The wind field changed by different wind bias reduction methods affected not only the smoke transport but also the fire spread direction and rate (Figure S18), emission time profile (Figure S19), as well as plume height at monitoring locations (Figure S20). Since the AICBC method effectively reduced the simulated wind speed, the burned area and emission rates from AICBC cases were lower than those of the other simulation cases. However, the AICBC without nudging case had a relatively high burned area and emission rates at 17:20 UTC (12:20 local time) on March 2nd. Although the AICBC case had a lower wind speed, wind direction also influenced the rate of fire spread and emissions. Because of the heterogeneous fuel distribution, differences in wind direction among the simulations caused the fire to burn different fuel types. Burned area rates were higher when fire spread to more flammable fuels, and emission rates were elevated when the fire consumed fuels that burned more quickly or had higher emission factors. The time profile of plume heights was more sensitive to the wind simulation compared to burned area and emissions (Figure S20). The plume heights at monitoring locations were influenced not only by the heat emitted from the fire but also by smoke transport. The plume heights varied depending on the relative position within the smoke plume, such as near the edge or along the centerline.

4.3. Smoke model evaluation methods

Wind bias reduction methods can improve wind simulations, but cannot eliminate all biases. However, addressing wind bias is essential before comparing smoke model simulations with observations. To account for the remaining wind bias, smoke model evaluation methods were implemented for properly assessing model performance. In smoke model evaluation methods, the temporal and spatial variation of wind bias must be addressed since the wind bias at the monitor (or assigned monitor) does not reflect the wind bias along the smoke trajectory. These methods considered the uncertainty of concentration due to the uncertain wind impacts, based on statistical sampling, which is represented as the gray shaded area in the figures of this section. In this study, we applied the smoke model evaluation methods to the nudging benchmark case (NB). However, the same methods, as post-analysis algorithms, can be combined with other wind bias reduction methods to improve the simulation performance and investigate the uncertain wind impacts on concentrations.

4.3.1. Rotation and translation

The rotation and translation method assumed the simulated concentration at the current hour would be affected mostly by the wind bias from the current hour and then the previous hour. If we applied the method considering only the current hour's wind bias, the concentration corrected for such wind bias could be estimated, which was indicated as the black dashed line in Fig. 5. We estimated the concentration uncertainty range by considering the wind bias from the current and previous hours using Eq. (1), which is shown as the shaded area in Fig. 5. The corrected concentration (black dashed line in Fig. 5) and the concentration uncertainty range (gray shaded area in Fig. 5 indicating the possible range of concentrations) estimated by the rotation and translation method showed a better performance compared to the nudging benchmark simulation (solid line in Fig. 5). The concentration uncertainty range indicated that it was possible to capture the observed $PM_{2.5}$ concentration peaks at Trailer FS during 17:00 to 19:00 UTC (12:00 to 14:00 local time) on March 3rd and 20:00 to 21:00 UTC (15:00 to 16:00 local time) on March 5th, at USFS 1079 during 19:00 to 21:00 UTC (14:00 to 16:00 local time) on March 2nd and 17:00 to 19:00 UTC (12:00 to 14:00 local time) on March 3rd, and at USFS 1078 during 17:00 to 20:00 UTC (12:00 to 15:00 local time) on March 2nd. However, the concentration uncertainty range had a lower concentration than the observations at Trailer FS on March 3rd. The peak timing at USFS 1078 on March 2nd was earlier than observed. This can be partly explained by the overestimation of wind speed in the simulation. Since we conducted translation operations based on the transport distance difference due to current and previous hour wind speed biases, the disparities in peak timing could be reduced, but still existed.

To understand the sensitivity of simulated concentration to wind direction and wind speed, we conducted a sensitivity analysis using rotation and translation operations as follows. We conducted −70 to +70 degrees perturbations on wind direction and 0 to 1.5 m/s perturbations on wind speed, which were the ranges suggested by the RMSE of NB (Tables S6 and S7). For each combination of wind direction and wind speed bias, we calculated the pseudo-monitor location for each monitor and extracted the concentration at that location. The sensitivity was calculated by taking the RMSEs between the simulated concentration time series at all pseudo-monitors and the corresponding observations (Figures S21-S23). The RMSE could exceed 80 $\mu g/m^3$ under the wind speed and wind direction bias range we selected, since the biased wind direction or wind speed could switch the monitor from smoke-impacted to not-impacted and vice versa, which would induce large differences in the $PM_{2.5}$ concentration.

4.3.2. Equal time and equal distance backward/forward trajectories

We used a similar convention as the RT method above; the uncertainty of concentration due to the wind bias was shown as the shaded area (Fig. 6), and the black dashed line indicated the concentration corrected by using the wind bias from the assigned meteorological monitor with the backward/forward trajectory methods. Since we estimated the uncertainty by a 1-sigma range of concentration intensity at pseudo-monitor locations rather than the maximum likelihood, the concentration corrected by the exact wind bias at the assigned monitor could be outside the range (for example, USFS 1078 on March 2nd in Fig. 6b). For the equal time backward/forward trajectory method (Fig. 6a), the likely concentrations (indicated by gray shaded area) covered the observed $PM_{2.5}$ concentration peaks at Trailer FS from 17:00 to 19:00 UTC (12:00 to 14:00 local time) on March 3rd, and the second peak from 20:00 to 21:00 UTC (15:00 to 16:00 local time) on March 5th, at USFS 1079 from 17:00 to 19:00 UTC (12:00 to 14:00 local time) on March 3rd, and at USFS 1078 on March 2nd from 17:00 to 20:00 UTC

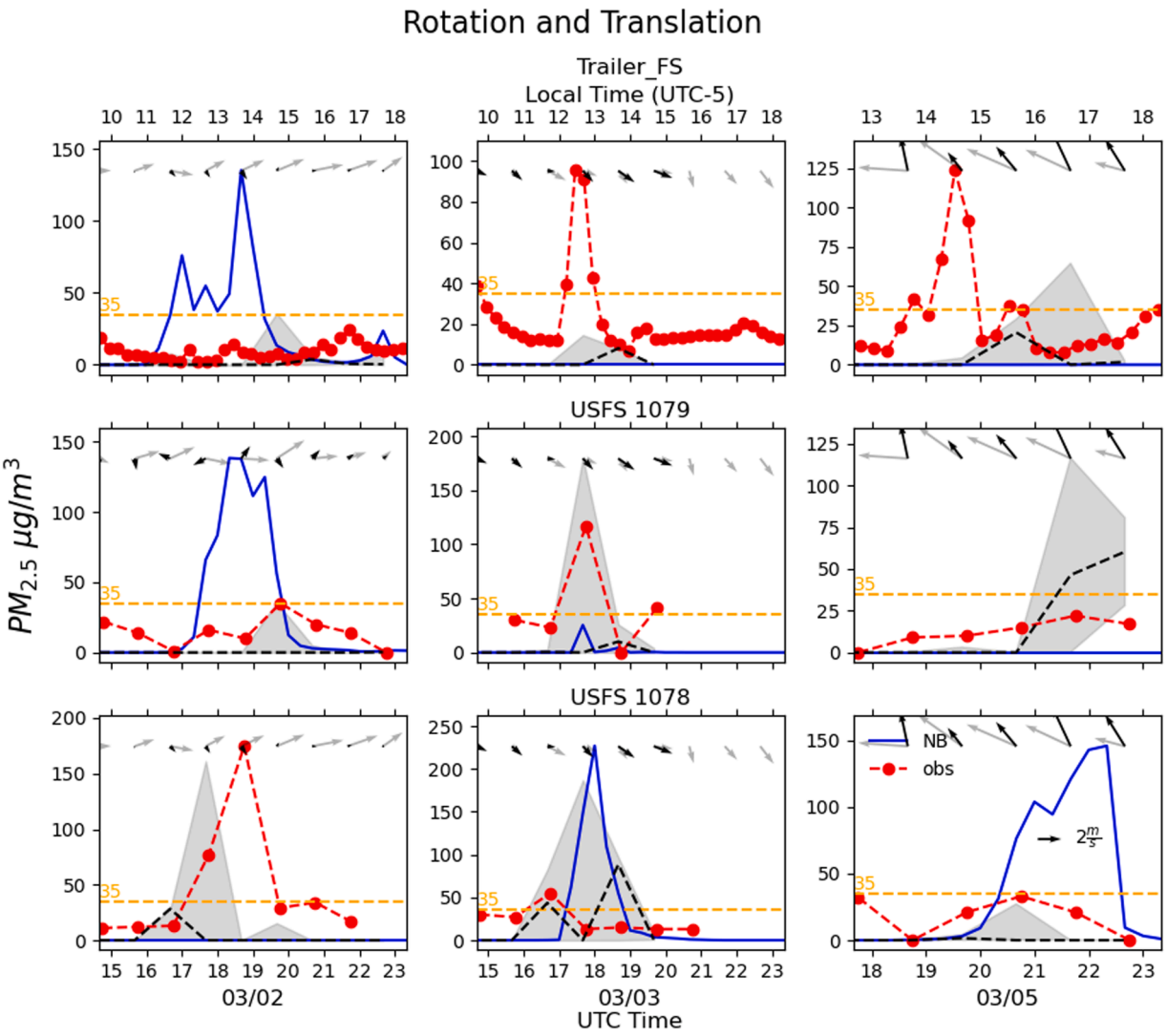

Fig. 5. Observed (red dots with dashed line), simulated (blue solid line), and corrected $PM_{2.5}$ (black dashed line) at Trailer FS (TEOM), USFS 1079 (EBAM), and USFS 1078 (EBAM) monitors on three prescribed fire days by using the RT method. The shaded area indicates the concentration uncertainty by considering the wind bias from the previous and current hours. The black and gray arrows at the top show the observed and modeled wind at the nearest meteorological monitor, respectively.

(12:00 to 15:00 local time). Also, the corrected $PM_{2.5}$ concentration (dashed black line) was lower during 16:00 to 20:00 UTC (11:00 to 15:00 local time) on March 2nd at Trailer FS and during 20:00 to 23:00 UTC (15:00 to 18:00 local time) on March 5th at USFS 1078 compared to the NB simulation (solid lines), displaying reduced concentration bias. The high $PM_{2.5}$ concentration at Trailer FS on March 3rd had a high probability of being captured by considering the wind bias, which was not captured in the RT method (Fig. 5). Additionally, the peak timing at USFS 1078 on March 2nd from the ETBFT method was closer to the measured smoke peak timing than the RT method. However, the shaded area in the ETBFT method suggested the probability of high $PM_{2.5}$ at Trailer FS and USFS 1079 on March 2nd, which were not observed, while the RT method did not indicate such smoke peaks. The enlarged shaded areas with ETBFT can be explained by the higher spatial variability of observed winds among the meteorological monitors. On that day, the USFS 1079 measured southwestern wind at 19:00 UTC (14:00 local time) while the gpem site reported northwestern wind (shown as observed Trailer FS wind vector on March 2nd). The ETBFT method considered the spatial and temporal variability of wind bias by simulating the smoke trajectories, while the RT method only considered the temporal variability of the wind during smoke transport (current hour and the previous hour) without considering the spatial variability.

For the equal distance backward/forward trajectory method (Fig. 6b), the concentration uncertainty range also showed the probability that the high $PM_{2.5}$ peaks could be captured at Trailer FS from 17:00 to 19:00 UTC (12:00 to 14:00 local time) on March 3rd, at USFS 1079 from 17:00 to 19:00 UTC (12:00 to 14:00 local time) on March 3rd, and at USFS 1078 on March 2nd from 17:00 to 20:00 UTC (12:00 to 15:00 local time). These two methods showed similar patterns since they conducted the same backward trajectory process to find the source of the smoke parcel. The difference was in the sampling of smoke along the forward trajectory. Both methods used trajectories calculated using the same simulated wind field, but they sampled concentrations at different times. The highest level of the shaded area in the EDBFT method was higher than the ETBFT method on March 5th for all three monitors. This was expected since the EDBFT method was designed to mitigate the dilution and diffusion effect due to the higher wind speed. The smoke was expected to be more concentrated with shorter transport distance due to less diffusion. However, the smoke concentration can be lower in EDBFT compared to ETBFT, as encountered on March 3rd at Trailer FS and USFS 1079. In ETBFT, the pseudo-monitors were located farther from the source because the forward trajectory distance, based on the overestimated wind speed from WRF, was longer than the backward trajectory distance. In contrast, EDBFT assumed equal forward and

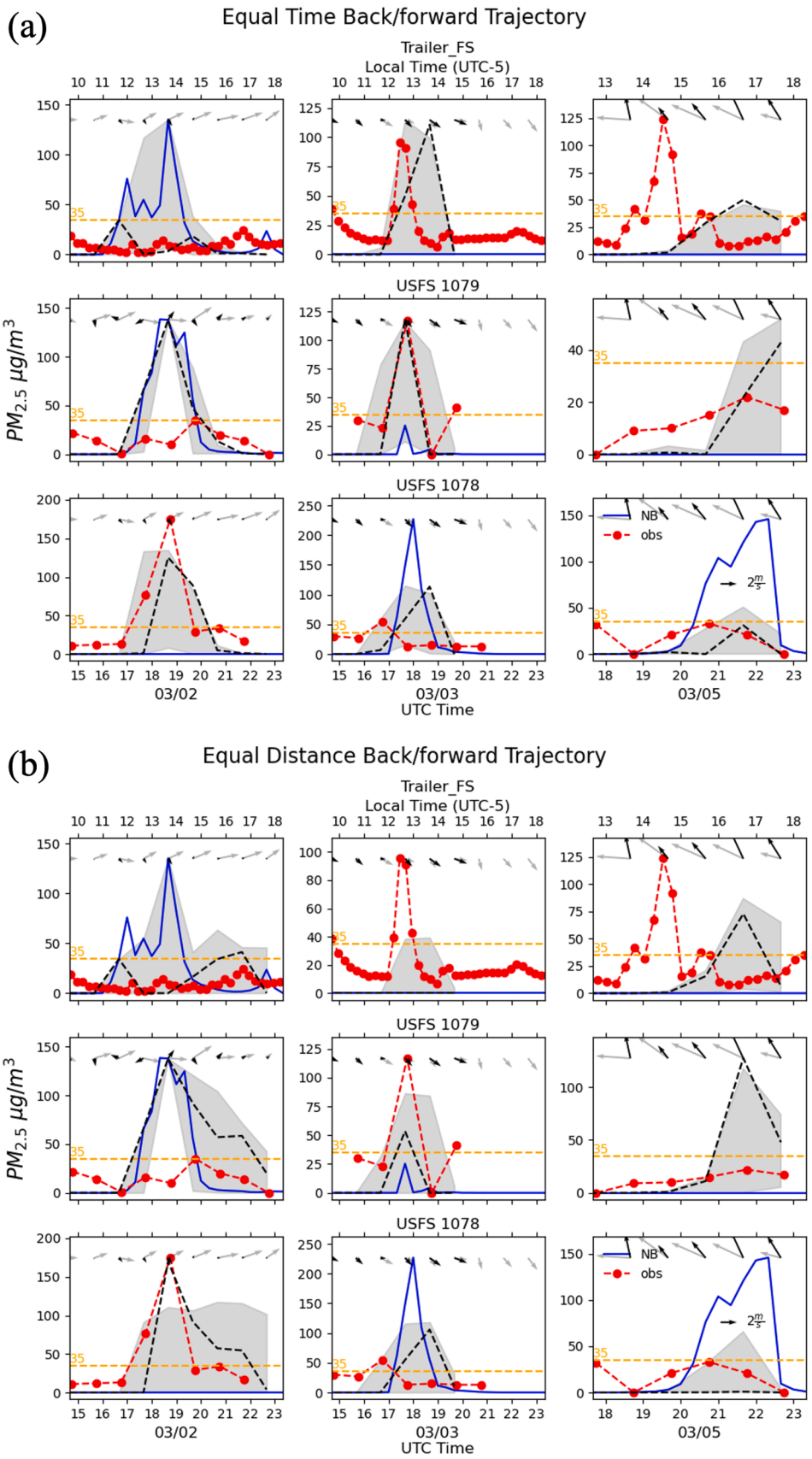

Fig. 6. Observed (red dot with dashed line), simulated (blue solid line), and corrected $PM_{2.5}$ (black dashed line) at TEOM monitor (Trailer FS), USFS 1079, and USFS 1078 on three prescribed fire days by using the ETBFT method (a) and the EDBFT method (b). The shaded area indicates the concentration uncertainty by considering the wind bias uncertainty along the trajectory. The black and gray arrows indicate the observed wind and modeled wind at the assigned meteorological monitor, respectively.

backward trajectory distances. Consequently, the higher plume rise near the source, caused by the elevation of fresh smoke with greater energy, leads to reduced surface concentrations at pseudo-monitors in EDBFT. This effect was particularly evident on March 3rd when these monitors were closer to the burn units than on other dates.

5. Discussion

The uncertainties from wind simulations highly impacted the $PM_{2.5}$ concentration field simulated by WRF-SFIRE. In this study, we showed that wind bias reduction methods can mitigate the wind simulation bias. Nudging to wind observations augmented through Kriging interpolation (i.e., the AN method) slightly improved the wind simulations; however, it did not improve the concentration simulations in the study cases (Figures S13). Although the nudging intensity could be increased by amplifying the magnitude of nudging artificial tendency terms in the settings, this was not done here since it may introduce unrealistic patterns in WRF simulations (Glisan et al., 2013). The AICBC method was the most effective method in reducing wind bias, particularly in addressing the overestimations of wind speed reported in many studies (Yu et al., 2022; Carvalho et al., 2014; Dzebre and Adaramola, 2020; Gholami et al., 2021; Jiménez and Dudhia, 2012; Pan et al., 2021; Carotenuto et al., 2020). Also, the smoke concentration simulation significantly improved with the winds simulated by the AICBC method. The improvements in concentration simulation could be partly explained by the reduced wind bias impacts on smoke transport, which was the main focus of this study. Moreover, the improved wind simulation also influenced the fire behavior simulation, such as the fire spread rate and direction, affecting the plume height, emission profile, and intensity (Figures S18-S20). These factors are critical for simulating smoke intensity, as higher fire spread rates, increased emissions, and/or lower plume heights can lead to higher ground-level smoke concentrations. The impacts of biased winds on these factors could be further investigated in future work, particularly if corresponding observations are available. Despite improving the wind simulation, the AICBC method still had limitations, and it could not eliminate all the wind bias at all monitors. In this method, we calculated an hourly bias by averaging all wind biases from all monitoring stations within the 1-km domain (WRF-SFIRE's parent domain). Then, the initial and boundary conditions were adjusted based on the averaged bias. The uniform adjustment for the whole domain effectively improved the simulation when a systematic error exists, such as the wind speed overestimation. However, the wind bias still existed in the initial conditions at the observed monitor locations after the correction, since the wind bias from different observations varied. For instance, the wind speed ratios between observations and WRF simulations were 0.25 and 0.11 at USFS 1079 and gpem, respectively, at 20:00 UTC (15:00 local time) on March 2nd. Since the AICBC method used the averaged wind bias, the initial conditions for wind speed at both monitoring locations were adjusted using the same scaling factor. The wind speed in the initial condition at gpem, although reduced, remains higher than the observations. To overcome such bottlenecks of the AICBC method, future studies could consider using wind fields generated through interpolation or data fusion (Chang et al., 2015; Wang et al., 2021) of the parent domain's wind field to provide initial and boundary conditions for the target nested domain. Another approach would be to use a meteorological model with higher spatiotemporal resolution, such as the High-Resolution Rapid Refresh model (HRRR), with the AICBC method to improve the ICBC used in WRF-SFIRE simulations. HRRR provides 3-km resolution meteorological data generated by a WRF simulation using data assimilation from various observational sources, including meteorological monitors, radar, satellite-based retrievals, and aircraft data (Benjamin et al., 2016). This plethora of data sources could potentially improve the simulation performance compared to the data assimilation configuration used in this study. Additionally, using HRRR to provide ICBC would reduce the computational costs by eliminating the need to downscale from 12 km to 4 km through WRF nesting. However, WRF simulations driven by HRRR ICBC would still have biases compared to observations, as noted in a previous study (Blaylock et al., 2017). These biases could potentially be mitigated through the AICBC method presented in this study.

For the smoke model evaluation methods developed in the study, the probability of high $PM_{2.5}$, which was not simulated in WRF-SFIRE, was estimated by considering the wind bias along the smoke transport trajectory. The RT method, which had the simplest physics assumptions, independently considered the bias from wind direction and speed, and corrected the biases by using rotation and translation separately. Since the method considered the wind uncertainty during the smoke transport by using observations from one meteorological monitor at current and previous hours, the method could be applied in scenarios where only one wind monitoring station provides data near the concentration monitor. This contrasts with the equal time or equal distance backward/forward trajectory methods, which require multiple wind monitoring stations to estimate the spatial variation in wind bias. However, using the two-hour wind bias to address the uncertainty during smoke transport is highly simplified. It could underestimate the uncertainty when the transport time is much longer and the wind spatial distribution variance is significant. The equal time or equal distance backward/forward trajectory methods considered the wind direction and speed bias simultaneously by estimating the trajectories of smoke under simulated and observed wind. Also, the transport time of the smoke was more accurately estimated by using the observed wind with the backward trajectory, rather than only considering the two-hour wind bias used in the RT method. Additionally, the spatial variations associated with the observational data used in backward trajectory calculation were addressed by the standard deviation of wind from multiple monitors. The ETBFT method estimated the uncertainties of smoke transport due to the wind bias, but had limitations in mitigating the dilution or diffusion effects from the wind speed bias. The EDBFT method was implemented as an alternative to overcome such limitations in the ETBFT method, assuming that the intensity of smoke diffusion was related to the smoke transport distance. In this study, ETBFT slightly outperformed EDBFT, particularly in capturing the concentration peak intensities at Trailer FS and USFS 1079 on March 3rd. Since the EDBFT used the backward trajectory distance to decide the forward trajectory distance, the destination time had to be rounded to match the simulation time resolution (i.e., 20 min in this study) for extracting the modeled concentration at the estimated pseudo-monitor location. In future studies, time interpolation of concentration could be considered to improve the implementation of the EDBFT method.

Accurately estimating the spatiotemporal differences between observed and simulated wind fields is critical for both the wind bias reduction and smoke model evaluation methods implemented in this study. However, the spatial sparsity of wind monitors introduces uncertainty in estimating wind biases within the simulation domain, thereby affecting the accuracy of these methods. To better understand the uncertainties associated with our methods, we conducted data withholding and sensitivity analyses for both wind bias reduction and smoke model evaluation methods. In wind bias reduction methods, we incorporated all available wind observations within the simulation domain to improve the modeled wind fields. However, this approach may lead to overestimated model performance because the same wind observations are used for both model adjustment and evaluation, which reduces the independence of the validation. To address this issue, we applied a data withholding strategy to assess the effectiveness of the AN and AICBC methods. Specifically, we withheld wind measurements from the gpem station, which is located within the WRF-SFIRE simulation domains for the March 2nd, 3rd, and 5th burns. The AN and AICBC methods were then applied, and the simulation results were evaluated using the withheld gpem wind data (Figure S27, Tables S8–S9). Compared to the benchmark simulation (B) that does not use gpem data either, the AN method improved wind direction simulation and showed

slight improvement in wind speed, while the AICBC method improved the simulation of both wind direction and wind speed, as indicated by the Taylor diagrams (Figure S27). The AICBC method remained the most effective, particularly in reducing wind speed bias, with the RMSE decreasing from 1.9 m/s to 0.7 m/s at the gpem station. For smoke model evaluation, recall that we quantified the uncertainty in predicted concentrations due to biases in simulated winds and showed this uncertainty as shaded areas in Figs. 5 and 6. When a concentration monitor was not co-located with a wind monitor, we assumed that the wind bias was the same as that of the nearest wind monitor. To evaluate the uncertainty associated with this assumption, we alternatively estimated the winds at concentration monitor locations using the inverse distance weighted (IDW) method on surrounding wind observations (Figures S28–S30). Compared to the gray shaded area predicted by the RT method using nearest-neighbor winds (Fig. 5), the RT method with IDW-estimated winds (Figure S28) better captured the $PM_{2.5}$ peak observed by Trailer FS at 18:00 UTC (13:00 local time) on March 3rd, but missed the peaks at USFS 1078 on March 2nd, 18:30 UTC (13:30 local time), and at Trailer FS on March 5th, 20:30 UTC (15:30 local time). For the ETBFT and EDBFT methods, using nearest-neighbor winds or IDW-estimated winds showed similar performance in capturing $PM_{2.5}$ peaks. As indicated by the black dashed lines, the ETBFT method using IDW-estimated winds shows better performance on predicting the $PM_{2.5}$ peak onset time at USFS 1078 on March 2nd, but performed worse on predicting the peak onset time at Trailer FS on March 3rd (Figure S29 and Fig. 6a). The EDBFT method using IDW-estimated winds slightly overestimated the magnitude of 18:30 UTC (13:30 local time) $PM_{2.5}$ peak at USFS 1078 on March 2nd (Figure S30 and Fig. 6b), as indicated by the black dashed lines. Overall, we found that the RT method was more sensitive to the choice of wind input than the ETBFT or EDBFT methods. Specifically, the RT method showed larger discrepancies between results using IDW-estimated winds and those using nearest-neighbor winds. This sensitivity arises because RT relies on a single wind observation site to estimate discrepancies in smoke transport trajectories under observed and simulated wind fields, whereas the ETBFT and EDBFT methods aggregate information from all available monitors in the simulation domain.

All simulation cases discussed in the study involve one burn unit (March 2nd and March 3rd) or two burn units next to each other (March 5th). In the discussions on smoke model evaluation methods, we simplified the smoke source to the centroid of the burn units. The RT method, which requires a center for the rotation operation, cannot simply be migrated to fire events when the burn units are far away from each other. The ETBFT and EDBFT methods, which use backward trajectories to identify the sources, can still be implemented under such situations. Additionally, the study mainly focused on uncertain wind impacts on ground-level concentration with limited discussion on fire emissions. However, fire emissions can play an important role in influencing surface concentration simulations in both fire behavior and chemical transport models. In fire behavior models, fire emissions' intensity and time profile can be affected by emission factors, fuel moisture, fuel type, and fuel load. Emission factors directly determine emissions' intensity but have a limited influence on fire behavior and therefore do not strongly affect the emission time profile. Based on the previous study (Prichard et al., 2020), the coefficient of variation (standard deviation divided by the mean) for prescribed fire $PM_{2.5}$ emission factors in the Southeastern U.S. ranges from 6 % to 63 %, depending on the fuel type, highlighting substantial uncertainty in current emission factors. Fuel moisture, fuel type, and fuel load affect fire propagation, which in turn affects emissions in fire behavior models. Fuel moisture was largely overestimated in WRF-SFIRE on March 5th, and the $PM_{2.5}$ peak at Trailer FS from 18:00 to 20:00 UTC (13:00 to 15:00 local time) on March 5th cannot be captured by either wind bias reduction or smoke evaluation methods. We applied WRF-SFIRE with reduced constant fuel moisture contents (of 11 %), and the emissions were more intense at the beginning time due to the faster fire spread rate (Figure S24). The smoke ($PM_{2.5}$) had a broader impact region (Figure S25) and a higher probability of hitting the monitor under wind uncertainty consideration with the ETBFT method (Figure S26). A previous study (Farguell et al., 2024) had suggested that fuel moisture reanalysis data, which incorporates RAWS fuel moisture observations with models, could improve fuel moisture simulation in WRF-SFIRE. Since the dataset was limited to California, it could not be used here; however, there is a potential benefit in adapting such reanalysis data with broader spatial coverage. We also conducted sensitivity analyses on the influence of fuel type and fuel load for the burn on March 5th (Table S10, Figures S31 and S32). For the fuel type sensitivity analysis, we replaced the heterogeneous fuel types derived from the 30-meter resolution LANDFIRE product with a single, uniform fuel type, either hardwood/long needle pine timber litter or tall grass. These two fuel types are dominant within the burn unit, accounting for 30 % and 27 % of the land cover, respectively. The burned area and emission time profiles are highly impacted by the fuel type. Fire propagated more quickly across tall grass and more slowly through hardwood litter. As a result, the simulation using tall grass as the fuel type shows an earlier $PM_{2.5}$ peak and higher maximum concentrations at the affected monitor location. In contrast, the hardwood fuel simulation showed a delayed $PM_{2.5}$ peak with lower intensity. For the fuel load sensitivity analysis, we conducted two additional simulations in which the fuel load for each fuel type was decreased or increased by 50 % compared to its value in the NB simulation. Fuel load influenced both burned area and emission time profiles. However, the burned area was relatively insensitive to changes in fuel load. Emissions are directly affected by fuel load, as they are typically calculated by the product of burned area, the consumed fraction of fuel load, and emission factors. As expected, the emissions are higher with increased fuel load and lower with decreased fuel load. The $PM_{2.5}$ concentrations from simulations with decreased or increased fuel load show similar temporal patterns, with all simulations reaching peak $PM_{2.5}$ levels around 22:00 UTC (17:00 local time). The increased fuel load simulation produced the highest peak $PM_{2.5}$ concentration, followed by NB, and then the decreased fuel load simulation. These differences in concentration levels can be explained by the emissions. When the burned area remains similar, a higher fuel load results in higher emissions and thus higher $PM_{2.5}$ concentrations. Another limitation of the study is that we only considered the uncertain surface wind simulation impacts on ground-level concentrations. However, the wind uncertainty in the mixing layer at higher elevations could also affect the ground-level smoke concentrations.

Data availability

The code related to wind bias reduction and smoke model evaluation methods is available on GitHub: https://github.com/zli867/CorrectiveWindSmoke (accessed on Feb 18, 2025). Other code and data related to the study will be made available upon request.

Disclaimer

The findings and conclusions in this publication are those of the authors and should not be construed to represent any official USDA or U. S. Government determination or policy.

Acknowledgements

This work was supported by the United States Army Corps of Engineers under Contract W912HQ-20-C-0019 to Georgia Tech Research Corporation for the Strategic Environmental Research and Development Program (SERDP) Project RC20–1047. Computational support was provided through the research cyberinfrastructure resources and services of the Partnership for an Advanced Computing Environment (PACE) at the Georgia Institute of Technology, Atlanta, Georgia, USA. We thank everyone who helped us with this work, especially the

authorities at Fort Stewart for hosting the field studies and their support in enabling our presence and field installations.

CRediT authorship contribution statement

Zongrun Li: Writing – review & editing, Writing – original draft, Visualization, Validation, Software, Methodology, Investigation, Formal analysis, Data curation, Conceptualization. **Susan M. O'Neill:** Writing – review & editing, Data curation, Conceptualization. **Rime El Asmar:** Writing – review & editing, Data curation. **Yongtao Hu:** Writing – review & editing, Software. **Adam K. Kochanski:** Writing – review & editing, Software. **Angel Farguell:** Software. **Jan Mandel:** Writing – review & editing, Software. **David J. Tanner:** Data curation. **L. Gregory Huey:** Supervision, Funding acquisition, Data curation. **Armistead G. Russell:** Supervision, Funding acquisition. **Rodney J. Weber:** Writing – review & editing, Supervision, Funding acquisition, Data curation. **M. Talat Odman:** Writing – review & editing, Validation, Supervision, Project administration, Methodology, Investigation, Funding acquisition, Formal analysis, Conceptualization.

Declaration of competing interest

The authors declare that they have no known competing financial interests or personal relationships that could have appeared to influence the work reported in this paper. The findings and conclusions in this publication are those of the authors and should not be construed to represent any official U.S. Department of Defense or U.S. Government determination or policy.

Supplementary materials

Supplementary material associated with this article can be found, in the online version, at doi:10.1016/j.agrformet.2025.110885.

References

Agency, U.E.P. The National Ambient Air Quality Standards for particle pollution, revised Air Quality Standards for particle pollution and updates to the Air Quality Index (AQI). 2012.

Beer, T., 1991. The interaction of wind and fire. Boundary Layer Meteorol. 54, 287–308.

Benjamin, S.G., Weygandt, S.S., Brown, J.M., Hu, M., Alexander, C.R., Smirnova, T.G., Olson, J.B., James, E.P., Dowell, D.C., Grell, G.A., 2016. A North American hourly assimilation and model forecast cycle: the Rapid Refresh. Mon. Weather. Rev. 144, 1669–1694.

Blaylock, B.K., Horel, J.D., Crosman, E.T., 2017. Impact of lake breezes on summer ozone concentrations in the Salt Lake valley. J. Appl. Meteorol. Climatol. 56, 353–370.

Bowden, J.H., Otte, T.L., Nolte, C.G., Otte, M.J., 2012. Examining interior grid nudging techniques using two-way nesting in the WRF model for regional climate modeling. J. Clim. 25, 2805–2823. https://doi.org/10.1175/JCLI-D-11-00167.1.

Burke, M., Childs, M.L., de la Cuesta, B., Qiu, M., Li, J., Gould, C.F., Heft-Neal, S., Wara, M., 2023. The contribution of wildfire to PM2. 5 trends in the USA. Nature 1–6.

Byun, D., Schere, K.L., 2006. Review of the governing equations, computational algorithms, and other components of the Models-3 Community Multiscale Air quality (CMAQ) modeling system. Appl. Mech. Rev. 59, 51–77.

Byun, D.W., Pleim, J.E., Tang, R.T., Bourgeois, A., 1999. Meteorology-chemistry interface processor (MCIP) for Models-3 Community Multiscale Air Quality (CMAQ) modeling system. Washington, DC, US Environmental Protection Agency. Off. Res. Dev.

Carotenuto, F., Gualtieri, G., Toscano, P., Miglietta, F., Gioli, B., 2020. WRF wind field assessment under multiple forcings using spatialized aircraft data. Meteorol. Appl. 27, e1920.

Carter, T.S., Heald, C.L., Jimenez, J.L., Campuzano-Jost, P., Kondo, Y., Moteki, N., Schwarz, J.P., Wiedinmyer, C., Darmenov, A.S., da Silva, A.M., 2019. How emissions uncertainty influences the distribution and radiative impacts of smoke from fires in North America. Atmos. Chem. Phys. Discuss. 2019, 1–50.

Carvalho, D., Rocha, A., Gómez-Gesteira, M., Santos, C.S., 2014. Offshore wind energy resource simulation forced by different reanalyses: comparison with observed data in the Iberian Peninsula. Appl. Energy 134, 57–64.

Center, W.R.C. USFS Remote automatic Weather station (RAWS) Data. 2008, 10.2602 3/9QFQ-P3MA-MB0E.

Chang, R., Zhu, R., Badger, M., Hasager, C.B., Xing, X., Jiang, Y., 2015. Offshore wind resources assessment from multiple satellite data and WRF modeling over South China Sea. Remote Sens. (Basel) 7, 467–487.

Chen, G., Guo, Y., Yue, X., Tong, S., Gasparrini, A., Bell, M.L., Armstrong, B., Schwartz, J., Jaakkola, J.J., Zanobetti, A., 2021. Mortality risk attributable to wildfire-related PM2· 5 pollution: a global time series study in 749 locations. Lancet Planet. Health 5, e579–e587.

Commerce., M.D.L.O.o.S.a.T.N.W.S.N.U.S.D.o. TDL U.S. and Canada Surface Hourly Observations. 1987.

Dennison, P.E., Brewer, S.C., Arnold, J.D., Moritz, M.A., 2014. Large wildfire trends in the western United States, 1984–2011. Geophys. Res. Lett. 41, 2928–2933.

Department of the Interior, G.S., and U.S. Department of Agriculture. LANDFIRE, 2016, Existing vegetation type layer, LANDFIRE 2.0.0. Available online: http://www.landfire/viewer (accessed on 1 May).

Diffenbaugh, N.S., Konings, A.G., Field, C.B., 2021. Atmospheric variability contributes to increasing wildfire weather but not as much as global warming. Proc. Natl. Acad. Sci. 118, e2117876118.

DRI. RAWS USA Climate Archive. Available online: https://raws.dri.edu/ (accessed on October 26, 2024).

Dzebre, D.E., Adaramola, M.S., 2020. A preliminary sensitivity study of Planetary Boundary Layer parameterisation schemes in the weather research and forecasting model to surface winds in coastal Ghana. Renew. Energy 146, 66–86.

El Asmar, R., Li, Z., Tanner, D.J., Hu, Y., O'Neill, S., Huey, L.G., Odman, M.T., Weber, R. J., 2024. A multi-site passive approach to studying the emissions and evolution of smoke from prescribed fires. Atmos. Chem. Phys. 24, 12749–12773. https://doi.org/10.5194/acp-24-12749-2024.

El Asmar, R., Li, Z., Yu, H., O'Neill, S., Tanner, D.J., Huey, L.G., Odman, M.T., Weber, R. J., 2025. Formation of ozone and PM2.5 in smoke from prescribed burning in the southeastern United States. ACS ES&T Air. https://doi.org/10.1021/acsestair.4c00231.

Ellison, L., Ichoku, C., Zhang, F., Wang, J., 2014. Building the fire energetics and emissions research (FEER) smoke emissions inventory version 1.0. In: Proceedings of the 2014 MODIS Science Team Meeting.

Emery, C.; Tai, E.; Yarwood, G. Enhanced meteorological modeling and performance evaluation for two Texas ozone episodes. Prepared for the Texas natural resource conservation commission, by ENVIRON International Corporation 2001, 161.

Emery, C., Liu, Z., Russell, A.G., Odman, M.T., Yarwood, G., Kumar, N., 2017. Recommendations on statistics and benchmarks to assess photochemical model performance. J. Air Waste Manag. Assoc. 67, 582–598.

Emery, C., Baker, K., Wilson, G., Yarwood, G., 2024. Comprehensive air quality model with extensions: formulation and evaluation for ozone and particulate matter over the US. Atmosphere (Basel) 15, 1158.

Farguell, A., Drucker, J.R., Mirocha, J., Cameron-Smith, P., Kochanski, A.K., 2024. Dead fuel moisture content reanalysis dataset for California (2000–2020). Fire 7, 358.

FIRMS, N. Fire information for resource management system. 2022.

Garcia-Menendez, F., Hu, Y., Odman, M.T., 2013. Simulating smoke transport from wildland fires with a regional-scale air quality model: sensitivity to uncertain wind fields. J. Geophys. Res. 118, 6493–6504.

Gholami, S., Ghader, S., Khaleghi-Zavareh, H., Ghafarian, P., 2021. Sensitivity of WRF-simulated 10 m wind over the Persian Gulf to different boundary conditions and PBL parameterization schemes. Atmos. Res. 247, 105147.

Giglio, L., Randerson, J.T., Van Der Werf, G.R., 2013. Analysis of daily, monthly, and annual burned area using the fourth-generation global fire emissions database (GFED4). J. Geophys. Res. 118, 317–328.

Glisan, J.M., Gutowski, W.J., Cassano, J.J., Higgins, M.E., 2013. Effects of spectral nudging in WRF on Arctic temperature and precipitation simulations. J. Clim. 26, 3985–3999.

Holmes, J.D., Paton, C., Kerwin, R., 2007. Wind Loading of Structures. CRC press.

Holmes, J., 2015. Wind Loading of Structures. CRC Press, Boca Raton.

Homer, C.H., Fry, J.A., Barnes, C.A., 2012. The national land cover database. US Geol. Surv. Fact Sheet 3020, 1–4.

Honnert, R., Efstathiou, G.A., Beare, R.J., Ito, J., Lock, A., Neggers, R., Plant, R.S., Shin, H.H., Tomassini, L., Zhou, B., 2020. The atmospheric boundary layer and the "gray zone" of turbulence: a critical review. J. Geophys. Res. 125, e2019JD030317.

Instruments, M.O. *E-BAM 9800 manual (Rev. P)*; Met One instruments: 2022.

Jaffe, D.A., O'Neill, S.M., Larkin, N.K., Holder, A.L., Peterson, D.L., Halofsky, J.E., Rappold, A.G., 2020. Wildfire and prescribed burning impacts on air quality in the United States. J. Air Waste Manage. Assoc. 70, 583–615.

Jiménez, P.A., Dudhia, J., 2012. Improving the representation of resolved and unresolved topographic effects on surface wind in the WRF model. J. Appl. Meteorol. Climatol. 51, 300–316.

Jolly, W.M., Cochrane, M.A., Freeborn, P.H., Holden, Z.A., Brown, T.J., Williamson, G.J., Bowman, D.M., 2015. Climate-induced variations in global wildfire danger from 1979 to 2013. Nat. Commun. 6, 7537.

Kaiser, J., Heil, A., Andreae, M., Benedetti, A., Chubarova, N., Jones, L., Morcrette, J.-J., Razinger, M., Schultz, M., Suttie, M., 2012. Biomass burning emissions estimated with a global fire assimilation system based on observed fire radiative power. Biogeosciences. 9, 527–554.

Kochanski, A.K., Jenkins, M.A., Yedinak, K., Mandel, J., Beezley, J., Lamb, B., 2016. Toward an integrated system for fire, smoke and air quality simulations. Int. J. Wildland. Fire 25, 534–546. https://doi.org/10.1071/WF14074.

Kochanski, A.K., Fournier, A., Mandel, J., 2018. Experimental design of a prescribed burn instrumentation. Atmosphere (Basel) 9, 296.

Kochanski, A.K., Mallia, D.V., Fearon, M.G., Mandel, J., Souri, A.H., Brown, T., 2019. Modeling wildfire smoke feedback mechanisms using a coupled fire-atmosphere model with a radiatively active aerosol scheme. J. Geophys. Res. 124, 9099–9116. https://doi.org/10.1029/2019JD030558.

Koster, R.D.; Darmenov, A.S.; da Silva, A.M. *The quick fire emissions dataset (QFED): documentation of versions 2.1, 2.2 and 2.4*; 2015.

Kumar, M., Kosović, B., Nayak, H.P., Porter, W.C., Randerson, J.T., Banerjee, T., 2024. Evaluating the performance of WRF in simulating winds and surface meteorology during a Southern California wildfire event. Front. Earth. Sci. (Lausanne) 11, 1305124.

Li, Y., Tong, D.Q., Ngan, F., Cohen, M.D., Stein, A.F., Kondragunta, S., Zhang, X., Ichoku, C., Hyer, E.J., Kahn, R.A., 2020. Ensemble PM2.5 forecasting during the 2018 Camp fire event using the HYSPLIT transport and dispersion model. J. Geophys. Res. 125. https://doi.org/10.1029/2020JD032768 e2020JD032768.

Liu, Y., Goodrick, S.L., Stanturf, J.A., 2013. Future US wildfire potential trends projected using a dynamically downscaled climate change scenario. For. Ecol. Manag. 294, 120–135.

Liu, T., Mickley, L.J., Marlier, M.E., DeFries, R.S., Khan, M.F., Latif, M.T., Karambelas, A., 2020. Diagnosing spatial biases and uncertainties in global fire emissions inventories: Indonesia as regional case study. Remote Sens. Environ. 237, 111557. https://doi.org/10.1016/j.rse.2019.111557.

Lu, W., Zhong, S., Charney, J., Bian, X., Liu, S., 2012. WRF simulation over complex terrain during a southern California wildfire event. J. Geophys. Res. 117.

Mallia, D.V., Kochanski, A.K., Urbanski, S.P., Lin, J.C., 2018. Optimizing smoke and plume rise modeling approaches at local scales. Atmosphere (Basel) 9, 166.

Mallia, D.V., Kochanski, A.K., Kelly, K.E., Whitaker, R., Xing, W., Mitchell, L.E., Jacques, A., Farguell, A., Mandel, J., Gaillardon, P.-E., et al., 2020a. Evaluating wildfire smoke transport within a coupled fire-atmosphere model using a high-density observation network for an episodic smoke event along Utah's Wasatch Front. J. Geophys. Res. 125. https://doi.org/10.1029/2020JD032712 e2020JD032712.

Mallia, D.V., Kochanski, A.K., Urbanski, S.P., Mandel, J., Farguell, A., Krueger, S.K., 2020b. Incorporating a canopy parameterization within a coupled fire-atmosphere model to improve a smoke simulation for a prescribed burn. Atmosphere (Basel) 11, 832.

Mandel, J., Beezley, J.D., Kochanski, A.K., 2011. Coupled atmosphere-wildland fire modeling with WRF 3.3 and SFIRE 2011. Geosci. Model. Dev. 4, 591–610.

Mandel, J., Amram, S., Beezley, J.D., Kelman, G., Kochanski, A.K., Kondratenko, V.Y., Lynn, B.H., Regev, B., Vejmelka, M., 2014. Recent advances and applications of WRF–SFIRE. Nat. Hazards Earth Syst. Sci. 14, 2829–2845. https://doi.org/10.5194/nhess-14-2829-2014.

Matz, C.J., Egyed, M., Xi, G., Racine, J., Pavlovic, R., Rittmaster, R., Henderson, S.B., Stieb, D.M., 2020. Health impact analysis of PM2. 5 from wildfire smoke in Canada (2013–2015, 2017–2018). Sci. Total Environ. 725, 138506.

Miller, C., O'Neill, S., Rorig, M., Alvarado, E., 2019. Air-quality challenges of prescribed fire in the complex terrain and wildland urban interface surrounding Bend, Oregon. Atmosphere (Basel) 10, 515.

Murphy, B.S., 2014. PyKrige: development of a kriging toolkit for Python. In: Proceedings of the AGU fall meeting abstracts. H51K-0753.

NCAR. NCEP ADP Global Upper air observational Weather data, October 1999 - continuing. 2004a, doi:10.5065/39C5-Z211.

NCAR. NCEP ADP Global Surface observational Weather Data, October 1999 - continuing. 2004b, doi:10.5065/4F4P-E398.

NCAR. NCEP North American Regional Reanalysis (NARR). 2005.

NCAR. NCEP North American Mesoscale (NAM) 12 km analysis. 2015a, doi:10.5065/G4RC-1N91.

NCAR. NCEP GDAS/FNL 0.25 Degree Global Tropospheric Analyses and Forecast Grids. 2015b.

Oliver, M.A., Webster, R., 1990. Kriging: a method of interpolation for geographical information systems. Int. J. Geogr. Inf. Syst. 4, 313–332.

Pan, L., Liu, Y., Roux, G., Cheng, W., Liu, Y., Hu, J., Jin, S., Feng, S., Du, J., Peng, L., 2021. Seasonal variation of the surface wind forecast performance of the high-resolution WRF-RTFDDA system over China. Atmos. Res. 259, 105673.

Potter, B., Yedinak, K., Charney, J., 2023. Measuring wind: creating new models to gauge impact on wildfire. Int. Assoc. Wildland Fire.

Prichard, S.J., O'Neill, S.M., Eagle, P., Andreu, A.G., Drye, B., Dubowy, J., Urbanski, S., Strand, T.M., 2020a. Wildland fire emission factors in North America: synthesis of existing data, measurement needs and management applications. Int. J. Wildland. Fire 29, 132–147.

Prichard, S.J., O'Neill, S.M., Eagle, P., Andreu, A.G., Drye, B., Dubowy, J., Urbanski, S., Strand, T.M., 2020b. Wildland fire emission factors in North America: synthesis of existing data, measurement needs and management applications. Int. J. Wildland. Fire 29. https://doi.org/10.1071/WF19066, 132-132.

Reen, B., 2016. A brief guide to observation nudging in WRF. Battlefield Environ. Divis., Army Res. Lab..

Rothermel, R.C. *A Mathematical Model For Predicting Fire Spread in Wildland fuels*; Intermountain Forest & Range Experiment Station, Forest Service, US …: 1972; Volume 115.

Schweizer, D., Cisneros, R., Shaw, G., 2016. A comparative analysis of temporary and permanent beta attenuation monitors: the importance of understanding data and equipment limitations when creating PM2. 5 air quality health advisories. Atmos. Pollut. Res. 7, 865–875.

Skamarock, W.C., Klemp, J.B., Dudhia, J., Gill, D.O., Liu, Z., Berner, J., Wang, W., Powers, J., Duda, M., Barker, D., 2019. A description of the advanced research WRF version 4. NCAR tech. note ncar/tn-556+ str 145.

Spero, T.L., Nolte, C.G., Mallard, M.S., Bowden, J.H., 2018. A maieutic exploration of nudging strategies for regional climate applications using the WRF model. J. Appl. Meteorol. Climatol. 57, 1883–1906.

Su, M., Shi, Y., Yang, Y., Guo, W., 2023. Impacts of different biomass burning emission inventories: simulations of atmospheric CO2 concentrations based on GEOS-Chem. Sci. Total Environ. 876, 162825.

Taylor, K.E., 2001. Summarizing multiple aspects of model performance in a single diagram. J. Geophys. Res. 106, 7183–7192.

Tian, D., Hu, Y., Wang, Y., Boylan, J.W., Zheng, M., Russell, A.G., 2009. Assessment of biomass burning emissions and their impacts on urban and regional PM2. 5: a Georgia case study. Environ. Sci. Technol. 43, 299–305.

Vejmelka, M., Kochanski, A.K., Mandel, J., 2016. Data assimilation of dead fuel moisture observations from remote automated weather stations. Int. J. Wildland. Fire 25, 558–568.

Wang, A., Xu, L., Li, Y., Xing, J., Chen, X., Liu, K., Liang, Y., Zhou, Z., 2021. Random-forest based adjusting method for wind forecast of WRF model. Comput. Geosci. 155, 104842.

Wiedinmyer, C., Akagi, S., Yokelson, R.J., Emmons, L., Al-Saadi, J., Orlando, J., Soja, A., 2011. The Fire INventory from NCAR (FINN): a high resolution global model to estimate the emissions from open burning. Geosci. Model. Dev. 4, 625–641.

Yang, E.S., Christopher, S.A., Kondragunta, S., Zhang, X., 2011. Use of hourly geostationary Operational Environmental Satellite (GOES) fire emissions in a Community Multiscale Air quality (CMAQ) model for improving surface particulate matter predictions. J. Geophys. Res. 116.

Yu, E., Bai, R., Chen, X., Shao, L., 2022. Impact of physical parameterizations on wind simulation with WRF V3.9.1.1 under stable conditions at planetary boundary layer gray-zone resolution: a case study over the coastal regions of North China. Geosci. Model. Dev. 15, 8111–8134. https://doi.org/10.5194/gmd-15-8111-2022.

Zachariassen, J. A review of the Forest Service remote automated weather station (RAWS) network. 2003.

Zhang, X., Bao, J.-W., Chen, B., Grell, E.D., 2018. A three-dimensional scale-adaptive turbulent kinetic energy scheme in the WRF-ARW model. Mon. Weather. Rev. 146, 2023–2045.